Catal Lett (2012) 142:399–407
DOI 10.1007/s10562-012-0780-x

Effect of Atomic Layer Deposition Support Thickness on Structural Properties and Oxidative Dehydrogenation of Propane on Alumina- and Titania-Supported Vanadia

Grigoriy Sereda · Christopher Marshall · Joseph A. Libera · James Dreessen · Anne Grady · Mark Turner

Received: 5 November 2011 / Accepted: 2 February 2012 / Published online: 22 February 2012

Abstract Engineered solid supports for vanadium catalysts were prepared by atomic layer deposition (ALD) of alumina and titania layers on silica. The thickness of these layers was found to have a significant effect on the structure of the solid supports, their interaction with vanadia, and their catalytic performance with regard to oxidative dehydrogenation of propane. The catalytic performance of supported vanadia catalysts is reported for both ALD-engineered and conventional solid supports (γ-Al_2O_3 and TiO_2). The analysis results indicated that the engineered supports behave as a separate phase rather than a cross between the base silica and the deposited alumina or titania.

Electronic supplementary material The online version of this article (doi:10.1007/s10562-012-0780-x) contains supplementary material, which is available to authorized users.

G. Sereda (✉) · J. Dreessen · A. Grady · M. Turner
Department of Chemistry, The University of South Dakota, 414 E. Clark St., Vermillion, SD 57069, USA
e-mail: gsereda@usd.edu

J. Dreessen
e-mail: jddreess@gmail.com

A. Grady
e-mail: Anne.Grady@usd.edu

M. Turner
e-mail: Mark.Turner@usd.edu

C. Marshall
Chemical Sciences and Engineering Division, Argonne National Laboratory, 9700 S. Cass Avenue, Argonne, IL 60439, USA
e-mail: Marshall@anl.gov

J. A. Libera
Energy Systems Division, Argonne National Laboratory, 9700 S. Cass Avenue, Argonne, IL 60439, USA
e-mail: jlibera@anl.gov

Keywords Heterogeneous catalysis · Catalysis · Alkanes · Mainly organic chemicals and reactions · TPR · UV

1 Introduction

Propene is one of the world's largest petrochemical commodities, particularly important in the synthesis of plastics and their precursors. Currently, there are two industrial processes for synthesizing propene from alkanes: catalytic cracking and catalytic dehydrogenation. Both processes are inefficient because they lead to high yields of coke and only small amounts of the desired alkene [1]. The oxidative dehydrogenation (ODH) of propane is a promising route for the synthesis of propene for several reasons. First, it is exothermic and, therefore, more energy efficient. Second, ODH of propane can be performed at lower temperatures (500 °C as compared to 800 °C for non-ODH). In addition, the major byproduct, water, can easily be separated from the alkene product. Finally, the presence of oxygen helps to circumvent carbon deposition on the catalyst. It has been documented in the literature that the best catalysts for the propane ODH are based on supported vanadium oxides [2].

Catalytic studies of vanadium oxide supported by ZrO_2, Al_2O_3, and SiO_2 for ODH of methanol and alkanes have shown that the nature of the solid support has a significant influence on the catalytic performance [3]. At low catalyst loadings (<0.52 V atoms/nm^2), vanadium oxide is more likely to be highly dispersed, forming isolated tetrahedral vanadate (V^{+5}) species after calcination in air. With increased loading, vanadium oxide species may form polymeric (dinuclear, trinuclear, etc.) two-dimensional networks of distorted tetrahedral and square-pyramidal oxovanadium clusters. At high loadings, three-dimensional

V_2O_5 crystallites in octahedral coordination become abundant [4]. Lewandowska et al. [5] have shown that the V–O-solid support bond is more significantly involved in the catalytic cycle of oxidation compared with V–O–V and V=O bonds. The dispersion of vanadium oxides in sub-monolayer to monolayer quantities depends on many parameters, such as nature of solid support [6], strength of support-vanadium oxide interactions, loading density of vanadium oxide precursors, and type of ligand attached to the vanadium atom [5, 7].

The distribution of the deposited vanadium oxide clusters over the surface of the solid support can be characterized by UV–Vis diffuse reflectance spectroscopy (DRS), based on the known quantitative dependence of the effective band gap energy on the number of vanadium atoms in the clusters [8]. Deconvolution of the UV–Vis DRS Kubelka–Munk function with Gaussian functions was introduced as an additional valuable tool for studying the nature of vanadium oxide and vanadate species on the surface of silica and mesoporous silica supports [9, 10]. The distribution of vanadium oxide deposited on zeolites was also studied by temperature programmed reduction (TPR) with H_2 [11]. Recently we found [12] that deposition of vanadates on solid supports in the presence of organic templates (phthalocyanine, calixarenes) does not change the extent of monovanadate polymerization, but affects interaction of vanadates with the solid support and, therefore, properties of the deposited catalysts.

In this paper we focus on the engineering of solid supports as a means of controlling catalytic performance of the deposited vanadates. Specifically, we report on the effect of the thickness of atomic layer deposition (ALD)-deposited alumina and titania layers on their structural properties and their performance as solid supports for the vanadia catalysts with regard to ODH of propane.

2 Experimental Section

2.1 Preparation of Catalysts

γ-Alumina (Sigma Aldrich Inc., 200 m^2/g), titania (BASF, 200 m^2/g), silica/alumina (319 m^2/g, Sigma Aldrich grade 135), ammonium metavanadate (99%, Aldrich, Inc.), and oxalic acid (EK Industries) were obtained from commercial sources. The conventional solid supports for impregnation (γ-alumina, silica/alumina, and titania) were dried in a 25–30 Torr vacuum at 100 °C overnight.

ALD was used to engineer Al_2O_3 and TiO_2 supports for vanadia catalysts. Thin films of alumina and titania were deposited on silica supports (Silicycle S10040M, 100 m^2/g) according to a known approach [13]. Briefly, in a single cycle of deposition, a metal precursor (trimethyl alumina or titanium tetrachloride) was first absorbed by partial hydrolysis with surface silica hydroxyls. After a purge period to remove unreacted metal precursor, the sample was then further reacted with water vapor to complete the hydrolysis and regenerate surface hydroxyl species, available for the next deposition cycle. One to 20 cycles of alumina and titania depositions were performed in 1 Torr of flowing UHP N_2 gas at 100 and 200 °C respectively. Each cycle added a thickness of approximately 1 Å of alumina or 0.5Å of titania on the silica. Vanadate was deposited on the corresponding solid support by using NH_4VO_3–$H_2C_2O_4$ as vanadate precursor, according to a known technique [14]. A vanadium loading of 2.5 V atoms/nm^2 was targeted (which should be less than monolayer coverage). The prepared materials were dried in air at 200 °C for 2 h and calcined in static air at 500 °C for 4 h.

2.2 Notation of Materials

In this manuscript, all catalysts are coded by a four component string. The first component denotes the chemical composition of the outer layer of the solid support ("A" for alumina, "T" for titania, and "S" for silica). The second and third components are assigned values from 1 to 20 according to the number of ALD layers, or designated "BL" for the bulk material. The fourth component is assigned "V" if vanadia is deposited, and "E" for empty solid supports. Thus, **A05E** stands for an empty solid support (no vanadium) with five ALD alumina layers, while **TBLV** stands for vanadia deposited on bulk titania. Bulk materials with different vanadium loads are additionally denoted by appended numbers (for instance, **ABLV-1** and **ABLV-2**).

The cross-section EDAX map (Fig. 1) of the **T20E** sample shows that the inner surface of the silica gel support was uniformly coated with titania.

2.3 Surface Analysis

Nitrogen adsorption–desorption studies were carried out at liquid N_2 temperature (77 K) with a NOVA 2200*e* series apparatus, and the results are reported in Table 1. The surface areas were calculated by the Brunauer–Emmett–Teller equation in the relative pressure range (P/P_0) of 0.05–0.30. The pore volume was determined from the amount of nitrogen adsorbed at the highest relative pressure of $P/P_0 \sim 0.99$. The pore diameter was calculated by applying the Barrett–Joyner–Halenda (BJH) equation to the adsorption isotherm. The samples were degassed at 100 °C for at least 1 h prior to the isotherm measurements.

The actual vanadium loadings were calculated on the basis of surface analysis of the final catalyst and are presented in Table 1.

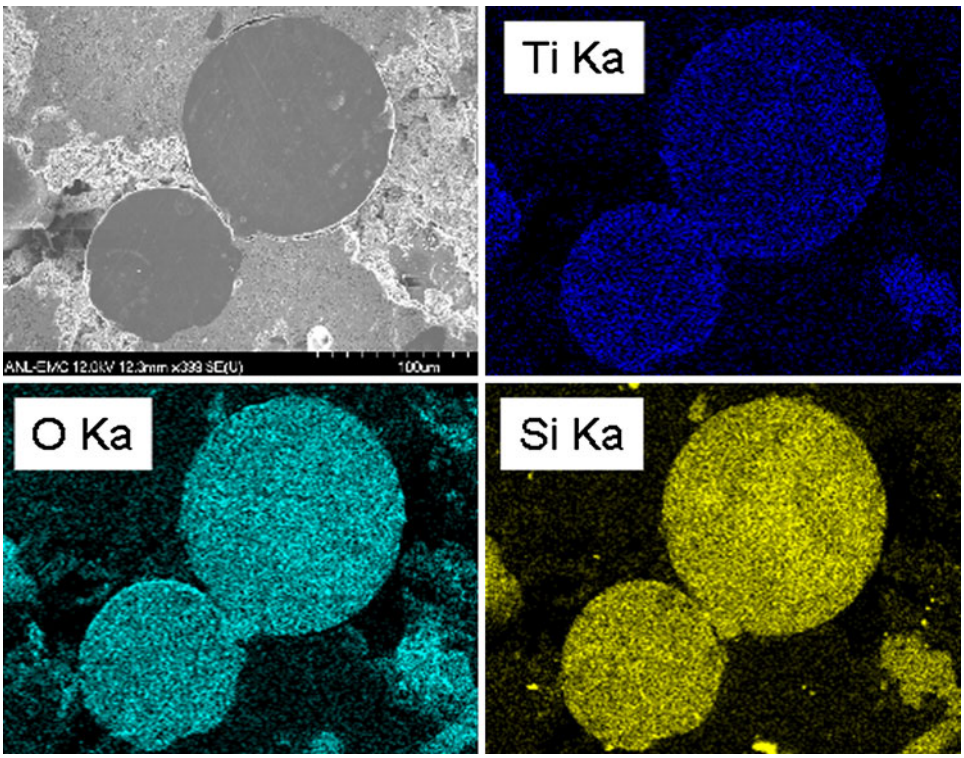

Fig. 1 EDAX maps of the material **T20**

2.4 Powder X-ray Diffraction

Powder X-ray diffraction (XRD) data for the catalysts were collected on a Siemens D5000 powder diffractometer using Cu $K\alpha$ radiation. Powder samples of 2 cm^3 were placed on a "zero background" holder slide, where petroleum jelly was used to keep the samples in place, and data were collected over the 2θ range of 5–80° using 0.02° steps. The resulting diffraction patterns collected were compared to standard patterns available in the JCPDS (Joint Commission of Powder Diffraction Standards) database.

2.5 Temperature Programmed Reduction

TPR was carried out in an Altamira system. Samples of ~40–90 mg were loaded into a quartz tube and calcined in air at 500 °C for 1 h. The samples were then cooled to room temperature in air (50 mL/min). The H_2 TPR profiles were monitored by flowing H_2–Ar gas (2.88% H_2/Ar) at a flow rate of 20 mL/min with a heating rate 8 °C/min in the temperature range 25–900 °C. The thermoconductivity detector (TCD) signal was recorded and plotted against temperature, and the sample was cooled to room temperature in helium. The temperature maxima determined from the TCD signals are summarized in Table 2.

2.6 UV–Vis DRS

Diffuse reflectance UV–Vis spectra were measured on a Varian-Cary 5000 UV–Vis-NIK spectrophotometer. The baseline was corrected for the bare support material, and the Kubelka–Munk function [15] was used to convert reflectance data into absorption spectra, which were deconvoluted with the Gaussian functions in the *Origin* software. Samples were kept at 150 °C overnight prior to analysis. The data were collected shortly after dehydration under ambient conditions. The DRS data are summarized in Table 3.

2.7 Steady-State Propane Oxidation

Steady-state propane oxidation was studied in a plug flow reactor. The catalysts were pre-treated in flowing 20% O_2/Ar (15 mL/min) at 150 °C for 2 h and 500 °C for 2 h. Propane (3% C_3H_8/Ar) and oxygen (20% O_2/Ar) were simultaneously passed through the reactor. The O_2:C_3H_8 molar ratio was adjusted to 2:1 by gas chromatography (GC) analysis. All catalysts were tested at 350, 400, 450, and 500 °C. Reactions were carried out in a quartz tube, and the reactor was packed with quartz wool above and below the catalyst bed. The catalyst bed temperature

Table 1 Surface characteristics of ALD samples before and after impregnation with vanadia

Material	Initial surface area (m^2/g)	Pore volume (mL/g)	Pore diameter (Å)	Vanadia coverage (V atoms/nm^2)	Weight after ALD (%)	Surface area (m^2/g)[a]
ABLE	200.0	1.40	–	0	–	–
ABLV-1	275.5	0.86	125	1.95	–	–
ABLV-2	270.7	0.88	130	4.57	–	–
ABLV-3	177.1	0.70	158	8.44	–	–
TBLE	200.0	0.77	–	0	–	–
TBLV-1	190.4	0.26	55	0.66	–	–
TBLV-2	56.5	0.16	121	8.85	–	–
SBLE	319.0	0.71	–	0	–	–
SBLV-1	345.6	0.45	48	3.72	–	–
SBLV-2	91.8	0.28	150	28.04	–	–
SBLV-3	58.7	0.21	177	65.77	–	–
A01E	92.1	–	–	0	102.9	94.8
A01V	109.1	0.44	177	2.12	–	112.3
A02E	92.9	–	–	0	105.0	97.5
A02V	102.4	0.74	291	1.83	–	107.6
A05E	90.9	–	–	0	108.9	99.0
A05V	123.4	0.59	197	1.83	–	134.4
A10E	78.5	–	–	0	121.8	95.6
A10V	150.1	0.47	126	1.66	–	182.8
A20E	59.9	–	–	0	146.9	87.9
A20V	202.9	0.39	65	1.22	–	298.1
T01E	100.4	–	–	0	103.2	103.6
T01V	94.8	0.78	329	2.60	–	97.8
T02E	100.9	–	–	0	105.2	106.2
T02V	97.4	0.69	298	2.60	–	102.5
T04E	105.3	–	–	0	113.4	119.4
T04V	92.0	0.65	302	3.26	–	104.3
T10E	108.97	–	–	0	126.9	138.3
T10V	86.9	0.58	279	3.51	–	110.3
T20E	118.85	–	–	0	167.3	198.9
T20V	74.8	0.36	207	4.61	–	125.2

[a] Specific surface area per 1 g of the base material before ALD

was maintained with a PID temperature controller and measured with a thermocouple in contact with the sample. The reaction products were analyzed using a TCD-equipped GC. For all samples the propane flow was maintained at 1.2 mL/min, and space velocity was 0.01 mol C_3H_8 (mol V s)$^{-1}$. The energy of activation and pre-exponential coefficient were calculated from an Arrhenius plot. The turnover frequency (TOF) was calculated based on the observed extent of propane conversion, surface area of the catalyst, and the vanadium load as follows:

$$\text{Conversion}\,(\%) = \frac{\#\ \text{of moles of}\ C_3H_8\ \text{consumed}}{\#\ \text{of moles of}\ C_3H_8\ \text{fed}} \quad (1)$$

$$\text{TOF}\,(s^{-1}) = \frac{\#\ \text{of}\ C_3H_8\ \text{molecules reacted}}{\#\ \text{of active sites} * s} \quad (2)$$

3 Results and Discussion

3.1 Surface Characteristics of Vanadia Supported by ALD Titania and Alumina

First, we explored how the number of ALD cycles and further impregnation of vanadia affect the surface of the deposited material. To offset the weight gain that occurs in the process of ALD, the specific areas of these samples were normalized to the weight of the original silica taken for the deposition. For instance, if a silica sample gained 3% of weight during ALD, the specific surface area was multiplied by 1.03.

As shown in Fig. 2, the specific surface area of ALD-deposited titania materials steadily rises with the number of

Table 2 Maxima of TPR peaks and vanadium loading for supported vanadia catalysts

Catalyst	First band maximum (°C)	Second band maximum (°C)	Third band maximum (°C)	Vanadia coverage (V atoms/nm^2)
ABLV-1	416	548	–	1.9
ABLV-2	428	545	–	4.5
SBLV-1	416	617	–	3.7
SBLV-2	387	623	–	28.0
SBLV-3	391	637	659	65.7
A01V	390	586	–	2.1
A02V	385	572	–	1.8
A05V	406	581	–	1.8
A10V	384	561	–	1.6
A20V	397	565		1.2
TBLV-1	342	400	–	0.6
TBLV-2	412	556 (Shoulder)	625	8.8
T01V	385	596	–	2.6
T02V	392	592	–	2.6
T04V	383	592	–	3.2
T10V	385	556	–	3.5
T20V	383	543 (Shoulder)	579	4.6

Table 3 Maxima of DRS peaks and vanadium loading for supported vanadia catalysts

Catalyst	First band maximum (nm)	Second band maximum (nm)	Third band maximum (nm)	Vanadia coverage (V atoms/nm^2)
ABLV-1	238	302	–	1.9
ABLV-2	248	293	–	4.5
ABLV-3	247	311	–	8.4
TBLV-2	243	309	–	8.8
SBLV-1	250	316	379	3.7
SBLV-2	245	323	436	28.0
SBLV-3	245	323	436	65.7
A01V	255	315	348	2.1
A02V	259	346	–	1.8
A05V	270	330	–	1.8
A10V	282	–	–	1.6
A20V	284	–	–	1.2
T01V	250	301	372	2.6
T02V	249	301	350	2.6
T04V	248	320	370	3.2
T10V	245	291	323	3.5

ALD cycles. It indicates that the deposited titania layer has added roughness with respect to the original silica surface possibly due to nanocrystalline morphology resulting in increased surface area. This tendency increases with the number of ALD cycles, which is consistent with the powder XRD patterns revealing crystallization of the deposited layers into anatase–TiO_2 (Fig. 3).

The XRD pattern of bulk TiO_2 (material **TBLE**) showed the presence of anatase phase only (Fig. 3). The material **T01V** with 1 ALD cycle of TiO_2 showed no crystallinity as opposed to its multilayer counterparts **T02V**, **T04V**, **T10V**, and **T20V**, where intensity of the anatase TiO_2 peaks (at $2\theta = 25$, 38, 48, 54, and 56°) gradually increased with each additional ALD layer. The presence of weak diffraction lines at 31 and 41° in the XRD pattern of **T20V** points to the formation of V_2O_5 crystals at the highest vanadium loading (6.8 atoms/nm^2) for this material. A very sharp peak at 50° and a set of smaller peaks at 33° belong

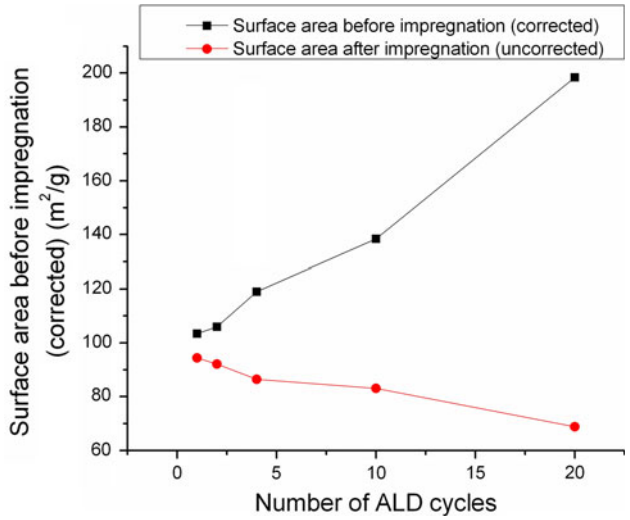

Fig. 2 Surface areas for ALD TiO_2 materials as function of number of ALD cycles before and after vanadia impregnation

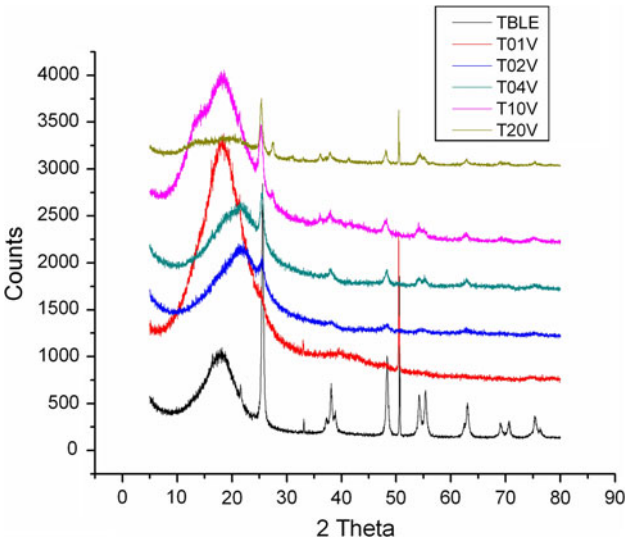

Fig. 3 Powder XRD patterns of ALD titania-supported vanadia

to quartz used as an internal standard. The intense peak at 18° belongs to petroleum jelly used for mounting the sample.

Further impregnation of vanadia decreases the surface area due to the known tendency of deposited vanadia to penetrate and fill micropores of the support material [6, 16]. This observation was independently confirmed by surface analysis of the alumina and silica supports impregnated with different surface densities of vanadia (Fig. 4). The tendency of the impregnated vanadia for filling the micropores is also consistent with the observed increase of the average pore diameter with the increased vanadium loading (see Table 1, series **ABLV-1** to **ABLV-3**, **SBLV-1** to **SBLV-3**, and **TBLV-1** to **TBLV-2**).

Interestingly, the ALD alumina series exhibits the opposite trend (Fig. 5). While deposition of Al_2O_3 layers does not seem to significantly affect the surface of the base silica, impregnation with vanadia induces a structural change in the material, leading to an increase in the surface area. This effect linearly increases with the number of ALD layers and does not tend to saturate even at 20 Al_2O_3 layers.

Since the vanadia coverage is inversely proportional to the surface area of the impregnated material, which is, in turn, significantly affected by the impregnation, it is very difficult to prepare a series of catalysts with the same vanadium loading. However, variations in the surface area and vanadium loading did not affect the arithmetical product of these parameters, allowing us to perform the catalyst performance study under consistent conditions.

3.2 Reducibility of Supported Vanadia by H_2

Deposition of the first ALD layer of Al_2O_3 on silica sharply decreases the temperatures of both reduction peaks for the supported catalysts (compared with the catalyst **SBLV-1**, supported by the base silica) by 20–40 °C; these peaks remain low throughout the whole series **A01V**–**A20V** (Table 2). This behavior is consistent with the fact that vanadia binds to the alumina support more strongly compared with silica, making the corresponding catalyst more active [17]. It is interesting that deposition of one Al_2O_3 layer covers the base silica well enough to completely suppress the TPR pattern of the **A01V** reduction peaks, a characteristic of the non-ALD catalyst **SBLV-1**. The influence of deposited vanadia on the structure of the solid support revealed by the specific surface area trends in the **A01V**–**A20V** series (Fig. 5) is consistent with the gradually

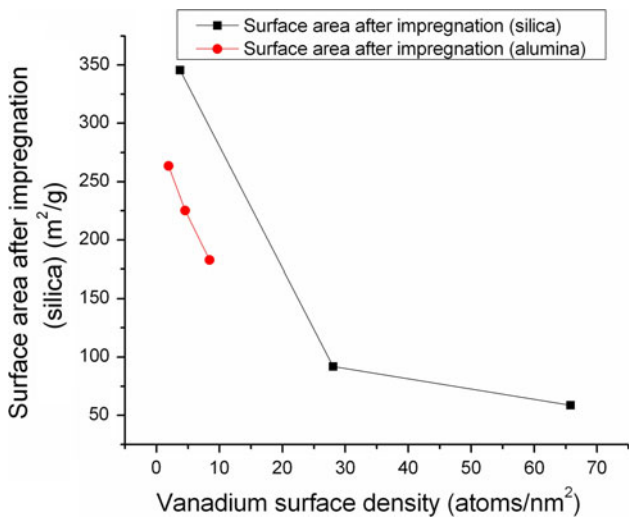

Fig. 4 Effect of the vanadia coverage on the surface area of alumina- and silica-supported materials

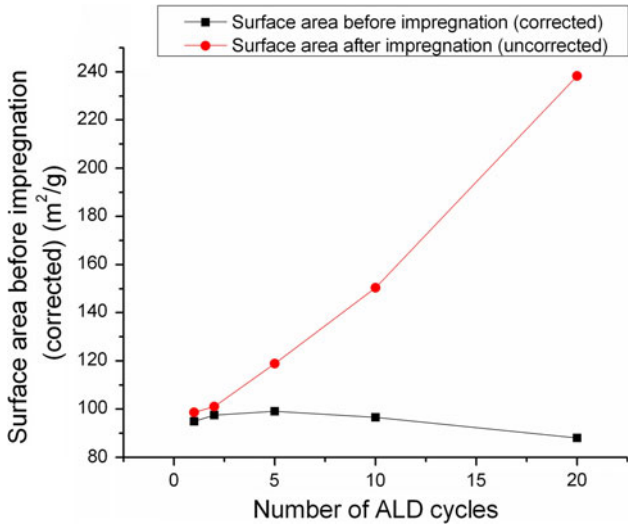

Fig. 5 Surface areas for Al_2O_3 materials as function of number of ALD cycles and vanadia impregnation

increasing intensity of the first reduction band with each additional ALD Al_2O_3 layer (Fig. 6).

The influence of vanadia deposited on the structure of the ALD TiO_2 support was not observed in the **T01V**–**T20V** series (Figs. 2, 7). As expected, the TPR patterns in this series approach those of the catalyst supported by the bulk TiO_2 with similar vanadium loading (Table 2; Fig. 7). Interestingly (Table 2), reducibility of the TiO_2-supported catalyst with a low vanadium load (**TBLV-1**, 0.66 V atoms/nm^2) is significantly higher than that for its higher vanadium-loaded counterpart (**TBLV-2**, 8.8 V atoms/nm^2).

3.3 Distribution of Vanadia over Conventional and ALD Solid Supports

According to the literature, supported vanadia catalysts include four types of vanadia species: (1) isolated surface VO_4 species containing one terminal V=O bond and three bridging V–O-support bonds, (2) polymeric surface VO_4 species containing one terminal V=O bond and three bridging V–O–V/V–O-support bonds, (3) crystalline V_2O_5 nanoparticles, and (4) mixed oxide supports at elevated temperatures (e.g., $AlVO_4$ and $V_xTi_{1-x}O_2$) [18]. We employed UV–Vis DRS to analyze distribution of vanadia [9, 10] over ALD-supported catalysts. The UV–Vis DRS spectra of samples **SBLV-1**–**SBLV-3** are typical for the distribution of impregnated vanadia over silica [9]. As the vanadium loading increases, the band in the 300–350 nm area (tetrahedral V–O–V oligomers) and in the 380–450 nm area (V–O–V polymers and octahedral crystallites) undergoes significant red shift, while the ligand-to-vanadium (isolated tetrahedral monovanadates) band at 250 nm remains unchanged (Table 3). Deposition of the first ALD Al_2O_3 layer on the silica does not significantly affect distribution of impregnated vanadia over different species. The only significant difference between UV–Vis DRS spectra for **A01V** and **SBLV-1** is a 29 nm blue shift of the 379 nm band, which may be attributed to the higher vanadium loading on the **SBLV-1** catalyst (Table 2). Therefore, significant suppression of the TPR peak at about 600 °C is likely due to the different binding of vanadia with the solid support rather than different distribution of vanadium between its surface species. However, we cannot rule out that part of vanadium is bound to the base silica that still might have been exposed. Deposition of each ALD Al_2O_3 layer gradually suppresses the 330–350 nm band (V–O–V oligomers), which is marginally present in the **A05V** material and is not evident for 10 and 20 ALD layers (**A10V** and **A20V**).

The UV–Vis DRS spectra of these materials exhibit only a band at about 280 nm. According to the literature [5], a single UV–Vis absorption peak in this area (ligand-to-vanadium charge transfer) points to the exclusive presence of isolated tetrahedral monovanadate on the surface. However, this maximum is significantly different from the 238 nm of vanadia impregnated in bulk alumina (**ABLV-1**,

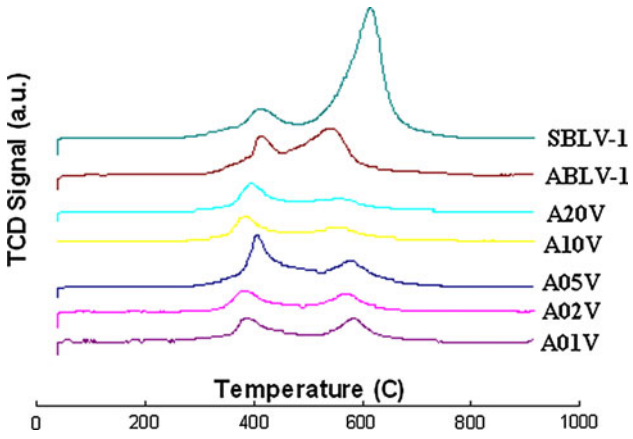

Fig. 6 TPR of vanadia impregnated into ALD Al_2O_3 supports

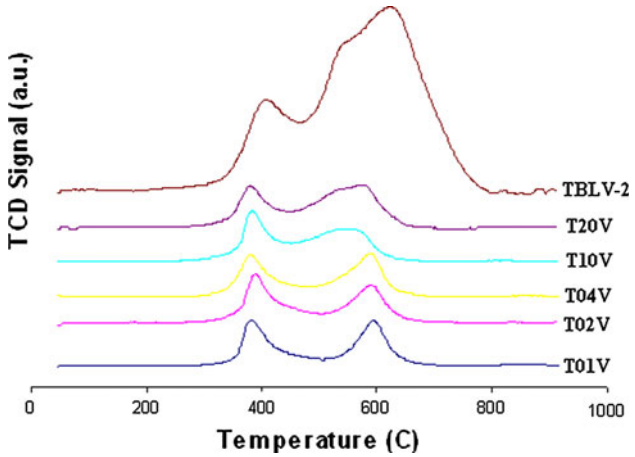

Fig. 7 TPR of vanadia impregnated into ALD TiO_2 supports

Table 4 Kinetic parameters of supported vanadia catalysts toward oxidation of propane

Catalyst	Activation energy (kJ/mol)	K_o	Vanadia coverage (V atoms/nm^2)	Conversion of propane at 450 °C (%)	TOF at 450 °C ($mol_{propene}/mol_V/s$)	Selectivity at 450 °C (%)		
						CO_2	CO	C_3H_6
SBLV-1	39.6	5.0×10^3	3.7	7	8.1×10^{-5}	81	10	9
A01V	151.7	1.3×10^{11}	2.1	2	3.9×10^{-5}	35	28	37
A02V	68.7	8.9×10^5	1.8	9	2.5×10^{-4}	63	18	19
A05V	111.2	9.5×10^8	1.8	9	3.3×10^{-4}	27	44	29
A10V	109.1	7.9×10^8	1.6	13	3.0×10^{-4}	35	42	23
A20V	117.3	2.8×10^9	1.2	11	2.3×10^{-4}	30	45	25
ABLV-1	133.0	7.8×10^{10}	1.9	21	7.6×10^{-4}	0	68	32
ABLV-2	77.85	1.2×10^7	4.5	36	3.4×10^{-4}	26	65	9
T01V	60.3	4.4×10^5	2.6	18	4.3×10^{-4}	24	60	17
T02V	89.9	7.3×10^7	2.6	22	5.5×10^{-4}	23	63	15
T04V	56.5	5.6×10^5	3.2	45	9.4×10^{-4}	26	67	7
T10V	38.2	4.9×10^4	3.5	55	3.2×10^{-4}	26	68	6
T20V	42.8	6.8×10^4	4.6	51	1.0×10^{-3}	24	71	5
TBLV-1	48.1	7.0×10^4	0.6	27	1.2×10^{-3}	96	4	0
TBLV-2	63.5	2.1×10^5	8.8	6	1.2×10^{-4}	70	14	16

Table 3). Therefore, the phase formed by 20 ALD layers of Al_2O_3 is different from that of the bulk Al_2O_3, which is consistent with the TPR data (Fig. 5). As expected [5], higher vanadium loadings on the bulk alumina led to the formation of polyvanadates, which exhibit a band in the 300 nm area, gradually growing and shifting toward lower energies as the loading increases (**ABLV-1**–**ABLV-3**, Table 3).

As opposed to Al_2O_3, TiO_2 significantly absorbs in the 200–300 nm area, which makes UV–Vis DRS impractical for the analysis of deposited vanadia species. Thus, anatase TiO_2 impregnated with vanadia at a relatively high loading (8.85 V atoms/nm^2, **TBLV-2**) exhibited the spectrum characteristic for bulk TiO_2 [19]. However, we observed a band of V–O–V oligomers over 320 nm in all ALD TiO_2 samples, with the intensity gradually subsiding as the number of ALD cycles increased from 1 to 10 (**T01V**–**T10V**, Table 3). In contrast, with the Al_2O_3 ALD series, deposition of TiO_2 does not suppress formation of the V–O–V oligomers of impregnated vanadia, while the TPR profiles become more similar to those of the bulk TiO_2-supported vanadia (Fig. 7).

3.4 Kinetics Parameters of Supported Vanadia Catalysts for the Oxidation of Propane

To ensure consistency of collected data, the catalytic measurements were made twice at each temperature and averaged. In addition, the whole catalysis performance experiment was repeated twice for **A05V**, and produced very similar results. Kinetics parameters and selectivity data are summarized in Table 4.

The propane oxidation data indicate that ALD deposition of the first Al_2O_3 layer drastically increases both activation energy and selectivity of the supported catalyst (**A01V**) toward formation of propene (from 9 to 37%). Deposition of the second layer increases reactivity of the catalyst and shifts its selectivity toward combustion. Further deposition of additional layers does not lead to any significant changes in the propane conversion and selectivity of the catalysts despite the gradual suppression of the 330–350 nm DRS band (corresponding to the V–O–V bond). However, neither structure nor properties of the ALD-prepared catalysts are not converging to those of the bulk Al_2O_3-supported counterpart (**ABLV**) as the number of the deposited layers increases. As expected, better selectivity toward propene was observed for lower propane conversions through the whole ALD series. Surprisingly, the **ABLV** catalyst demonstrated higher propene selectivity even at a higher propane conversion. Further, contrary to the ALD-catalysts, no CO_2 was observed on the **ABLV** catalyst. While the mechanistic details of the oxidation process remain unclear, different catalytic performance of Al_2O_3-supported catalysts at 1–2 V/nm^2 is more likely to be linked to the different modes of binding between the deposited vanadate species with the solid support rather than to their extent of polymerization. This is consistent with the strong binding between vanadates and the solid support (evidenced by lower temperatures of the H_2-TPR reduction peaks [17]) and the known [20] presence of

different binding sites on the surface of Al_2O_3. The different mode of binding between deposited monovanadate and the bulk Al_2O_3 support is also consistent with the significant shift of the first DRS band (238 nm) with respect to the ALD series (250–280 nm).

Similarly, in the ALD TiO_2 series, the 1 ALD catalyst (**T01V**) is as selective toward propene as the bulk TiO_2-supported catalyst (**TBLV-2**), but at much higher propane conversion (Table 2). Since another reference material with low vanadium loading (**TBLV-1**) leads to 100% combustion (Table 4), the **T01V** surpasses both bulk TiO_2-supported counterparts for conversion of propane to propene. Deposition of each additional TiO_2 layer gradually increases reactivity (TOF) and decreases selectivity of the supported catalysts toward propene. Thus, kinetic parameters of the ALD series do not approach those of the bulk TiO_2-supported catalyst, but rather drift in the opposite direction. Similarly to the Al_2O_3 series, ALD TiO_2-supported catalysts exhibit higher propene selectivity at lower propane conversions with their bulk-supported counterparts being outside of this trend. Interestingly, according to the UV–Vis DRS results, the distribution of vanadia between various surface species is not significantly different for the whole ALD TiO_2 series, which confirms the primary role of the V–O-solid support bond [6] in the process of catalytic oxidation.

4 Conclusion

ALD of Al_2O_3 and TiO_2 on silica-coated alumina leads to the formation of phases different from those of the bulk oxides. The ALD Al_2O_3 structure is significantly affected by impregnated vanadia, while its influence on the ALD TiO_2 structure is less prominent. In contrast with the Al_2O_3, ALD deposition of TiO_2 does not suppress formation of V–O–V oligomers of impregnated vanadia. The number of ALD TiO_2 layers significantly affects catalytic performance of the supported vanadia, but not the distribution of vanadium between different surface species. This finding confirms the primary role of the V–O-solid support bond in the process of catalytic oxidation of propane and demonstrate importance of engineering of solid supports for the design of new catalysts.

Acknowledgments This work has been supported by the Director, Office of Science, Office of Biological and Environmental Research, Biological Systems Science Division of the US Department of Energy under Contract No. DE-FG02-08ER64624; by the National Science Foundation (NSF-CHE-0722632, EPSCoR Grants No. 0554609 and 0903804), and by the State of South Dakota (NSF NPURC Grant 0532242). Christopher L. Marshall and Joe Libera acknowledge the support of the US Department of Energy, Office of Basic Energy Science under Contract DE-FG02-03-ER15457.

References

1. Cavani F, Vallarini N, Cericola A (2007) Catal Today 127:113
2. Lemonidou AA, Nalbandian L, Vasalos IA (2000) Catal Today 61:333
3. Ertl G, Knözinger H, Weitkamp J (eds) (1999) Preparation of solid catalysts. Wiley VCH, Weinheim
4. Arena F, Giordano N, Parmaliana A (1997) J Catal 166:66
5. Lewandowska AE, Banares MA, Khabibulin DF, Lapina OB (2009) J Phys Chem C 113:20648
6. Gao X, Wachs IE (2000) J Phys Chem B 104:1261
7. Arena F, Fusteri F, Parmaliana A (1999) Appl Catal 176:177
8. Conforth JW, Morgan ED, Potts KT, Rees RJW (1973) Tetrahedron 29:1659
9. Baltes M, Cassiers K, Van Der Voort P, Weckhuysen BM, Schoonheydt RA, Vansant EF (2001) J Catal 197:160
10. Capek L, Adam J, Grygar T, Bulanek R, Vradman L, Kosova-Kucerova G, Cicmanec P, Knotek P (2008) Appl Catal A 342:99
11. Roozeboom F, Miltlermeljer-Hazeleger MC, Moulljn JA, Medema J, de Beer VHJ, Gellings PJ (1980) J Phys Chem 84:2783
12. Sereda G, Kim T, Jones A, Khatri H, Marshall C, Subramanian H, Koodali R (2011) Catal Lett 141:1086
13. George SM, Ott AW, Klaus JW (1996) J Phys Chem 100:13121
14. Reddy EP, Varma RS (2004) J Catal 221:93
15. Argyle MD, Chen K, Bell AT, Iglesia E (2002) J Catal 208:139
16. Concepcion P, Reddy BM, Knözinger H (1999) Phys Chem Phys 1:3031
17. Magg N, Immaraporn B, Giorgi JB, Thomas S, Baumer M, Dobler J, Wu Z, Kondratenko E, Cherian M, Baerns M, Stair PC, Sauer J, Freund H (2000) J Catal 226:88
18. Tian H, Ross EI, Wachs IE (2006) J Phys Chem 110:9593
19. Park S-J, Kang YC, Park JY, Evans EA, Ramsier RD, Chase GGJ (2010) Eng Fibers Fabr 5:50
20. Kim HS, Zygmunt SA, Stair PC, Zapol P, Curtiss LA (2009) J Phys Chem C 113:8836